ITER BASELINE SCENARIO INVESTIGATIONS ON TCV AND COMPARISON WITH AUG

O. SAUTER, M. VALLAR, B. LABIT, A. KARPUSHOV, F. BAGNATO, S. CODA, A. MERLE,
École Polytechnique Fédérale de Lausanne, Swiss Plasma Center
1015 Lausanne, Switzerland
E-mail: Olivier.Sauter@epfl.ch

T. PÜTTERICH, V. BOBKOV, M.G. DUNNE, P.T. LANG, M. MARASCHEK, R.M. MCDERMOTT, PH. NEUBERT, J. STOBER, W. SUTTROP, M. WILLENSDORFER
Max-Planck-Institut für Plasmaphysik,
85748 Garching, Germany

I. VOITSEKHOVITCH,
EURATOM/CCFE Fusion Association, Culham Science Centre
Abingdon OX14 3DB, UK

Y. CAMENEN, F. WIDMER
CNRS, Aix-Marseille Univ., PIIM UMR7345
Marseille, France

F. ERIKSSON, E. FRANSSON
Chalmers University of Technology
Gothenburg, Sweden

M. MANTSINEN,
Barcelona Supercomputing Center (BSC), Barcelona, Spain; ICREA
Barcelona, Spain

TCV TEAM
See author list of "H. Reimerdes et al this conference and S. Coda et al 2019 Nucl. Fusion 59112023"

ASDEX UPGRADE TEAM
See author list of "H. Meyer et al. 2019 Nucl. Fusion 59 112014"

EUROFUSION MST1 TEAM
See author list of "B. Labit et al 2019 Nucl. Fusion 59086020"

Abstract

Under the auspices of EUROfusion (WPMST1), the ITER baseline scenario (IBL, [1]) is jointly investigated on AUG and TCV. While the AUG results were presented at the last IAEA FEC [2], this contribution focuses on the recent results obtained in TCV and related integrated modelling results. Such developments in TCV were only possible with the installation of an NBI heating source [3], allowing ELMy H-modes at ITER relevant β_N. The IBL scenario is mainly characterized by low q_{95} (3.0-3.6), high positive triangularity (δ>0.35) and relatively high elongation (κ>1.65) and normalized beta (β_N>1.5). In AUG, these combinations lead to very steep and narrow edge transport barriers, when good confinement is obtained, with high pedestal pressure and therefore large type-I ELM crashes. A similar behaviour is also observed on TCV where discharges with similar confinement properties (H_{98}~1) and normalized beta (β_N~1.8), as those expected for the ITER baseline scenario, have been obtained. TCV IBL performance is mainly limited by (neoclassical) tearing modes, in particular 2/1 modes. We show that they can be avoided with central X3 EC heating at relatively high q_{95} and moderate β_N. However, the lack of significant ECH at the high central densities obtained in TCV IBL scenario limits the duration of low q_{95} cases to about six confinement times. During this time, current density can fully evolve and density usually keeps peaking until (neoclassical) tearing modes are triggered. Integrated modelling results show ITG dominant instabilities in both AUG and TCV IBLs, and show that, in TCV, NBI fuelling also plays a role to sustain the mainly turbulent-driven significant peaked density profiles. The role of profiles, sawteeth and ELMs regarding MHD stability are also discussed. Safe termination of AUG IBL is demonstrated, q_{95}~3 included, consistent with predictive optimization using RAPTOR.

1. INTRODUCTION

The ITER baseline scenario (IBL) is being studied in various tokamaks (IBL, [1]). It is the inductive ELMy H-mode "standard" scenario aiming for Q=10 performance in ITER [4]. The main recent AUG results have been

detailed at the last IAEA conference [2] and we focus here on the developments of the TCV IBL based on the know-how obtained at AUG. TCV results and analyses are then used to test further IBL in AUG. TCV recently installed an NBI heating source [3], allowing ELMy H-modes at ITER relevant β_N. The IBL scenario is based on the confinement improvement of ELMy H-modes with increasing positive triangularity, thanks to an increase of the average top pedestal pressure ([1], [4]) through an improved edge stability. Note that the ITER triangularity is very high (table 1, Fig. 1), near 0.5, and is at the top of the highly sensitive dependence of pedestal top pressure versus triangularity as shown in Fig. 10 of Ref. [5]. It is shown that a change of δ_{av} from 0.3 to 0.5 can almost double the predicted pedestal pressure. Using its higher shaping flexibility compared to AUG, the ITER baseline shape in TCV is in between the AUG one and the so-called ITER scenario 2. First, we focused on reproducing the AUG shape, for comparison, and then increasing further triangularity and elongation towards scenario 2. However ITER parameters have not been reached yet due to MHD instabilities as will be discussed later. We define the IBL with low q_{95}, aiming for q_{95}=3 as the ITER scenario 2 reference, high β_N, high elongation, aiming for κ=1.8 and high Greenwald fraction (although low collisionality is also interesting to investigate core and pedestal properties).

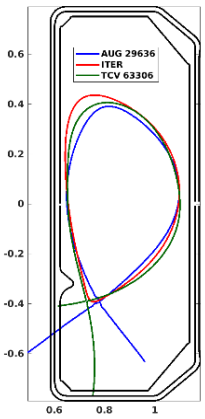

TABLE+Fig 1. ITER baseline shape main parameters (and rescaled shapes to match TCV vessel)

	AUG 29636@4s	TCV 63306@1.2s	ITER Scen 2
delta top	0.25	0.28	0.49
delta bottom	0.40	0.61	0.50
delta avg	0.33	0.44	0.50
kappa	1.73	1.78	1.84

We first discuss the operating range of the TCV IBL discharges and compare with AUG results. We will then focus on the role of MHD and demonstrate how β_N, q_{95} and profiles play a role, using X3 central heating. We also present the developments of a safe termination of AUG IBL scenarios, using predictive optimization simulations. Finally, we shall discuss heat and particle integrated modelling, using ASTRA-GLF23 and GENE.

2. ITER BASELINE SCENARIOS IN AUG AND TCV

The main figures of merit are the H_{98} scaling factor and normalized pressure β_N [1]. As discussed in [2], AUG has focused on two IBL scenarios with q_{95}~3 and q_{95}~3.6 (Fig. 2). In both cases, large type I ELMs occur and lead to significant perturbations, which are more severe with lower q_{95} (higher I_p actually), hence the developments at q_{95}~3.6. The constant dashed lines represent constant H_{98}/β_N values with similar performance properties if $q_{95} \propto \beta_N$ (cst $H_{98}\beta_N/q_{95}^2$). They also reflect the observed confinement improvement with β_N not included in H_{98}. AUG IBL with carbon wall had better confinement properties [6] and spanned the region at and above the ITER point (β_N=1.8;H_{98}=1), and its alternative with similar performance (2.2;1.2). As seen in Fig. 2, with tungsten walls, this is recovered only at lower collisionality, despite being obtained with edge density pump-out thanks to magnetic perturbations (MP) [7]. To contribute to further developments at lower q_{95}, a successful new 2nd harmonic ICRH H heating scheme has been developed and tested [8], which will allow lower B_0, I_p scenarios for better MP effects.

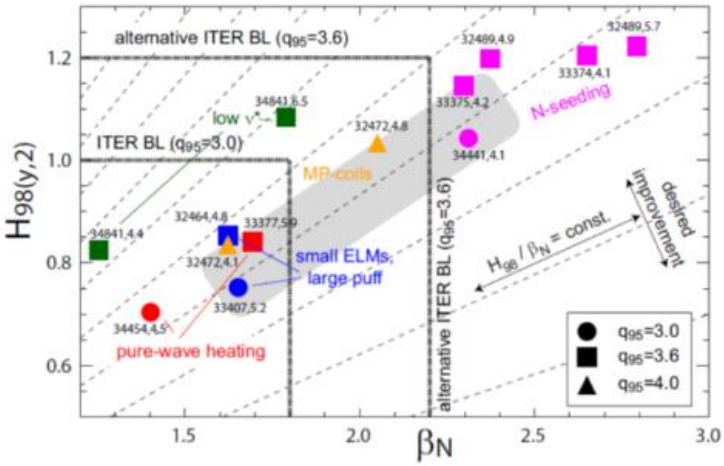

FIG. 2: *AUG IBL results as reported in Ref. [2]. With W wall, note that only the low collisionality points follow a trend with better confinement properties than required for ITER Q=10*

The TCV IBL results are reported in Fig. 3 including the pedestal top values for electron temperature and density, following the definitions in [9] (Fig. 3b). In Fig. 3a it is interesting to note that the data points align relatively well with slightly better confinement properties than the required ITER target, consistent with previous carbon wall studies [1, 6] and also exhibit ~cst H_{98}/β_N properties. TCV IBL span about a factor of two in pedestal pressure, although most points are at about 2kPa the confinement improvement with β_N at high f_G is consistent with an increase of $n_{e,ped}$ at constant $T_{e,ped}$. The higher density cases tend to follow the lower confinement dashed line, combined with lower q_{95}, while the higher confinement points tend to have higher q_{95} and lower f_G.

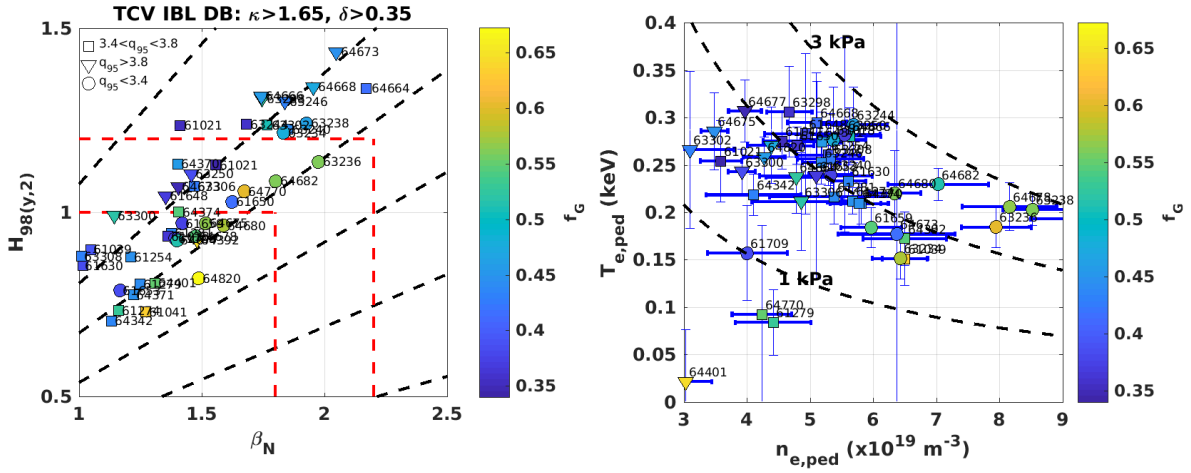

FIG. 3: *TCV IBL results with 1.65<κ<1.78 and 0.35<δ_{av}<0.44. (a) H_{98} vs β_N according to the Grennwald fraction f_G. (b) Pedestal top values for electron temperature and density following [9]*

One expects confinement degradation at higher Greenwald fraction from previous studies [1 and refs therein], which is usually alleviated by increasing the edge triangularity. Fig. 4 shows H_{98} vs f_G for the full TCV database of "ITER" like shapes, including smaller elongation and triangularity. TCV data is consistent with the trend described in [1] with a maximum H_{98} factor around 1.5 for f_G~0.4 and about 1 for f_G~1. However the points near this trend are not at the highest δ values, but rather have smaller elongation. This is related to the consistent experimental observation on TCV that ELMy H-modes are much more reliable at lower elongation and less perturbed by type I ELMs. Note that TCV triangularities, especially near the X-point, are on the high side in any case, which might explain why we can observe the effect of elongation which has a larger variation. Note also that the effective TCV density limit is usually below f_G~1. Higher elongation leads to naturally lower internal inductance l_i and broader current density profiles [10], which can explain a lower density limit or higher sensitivity to density peaking for triggering 2/1 modes in particular. This is consistent with the important role of the slow time evolution of the current density profile shown in DIII-D IBL [11] and consistent with the role of both global q profile and increase magnetic shear near q=2 on tearing mode stability observed on TCV and included in a varying Δ' within the modified Rutherford equation [12].

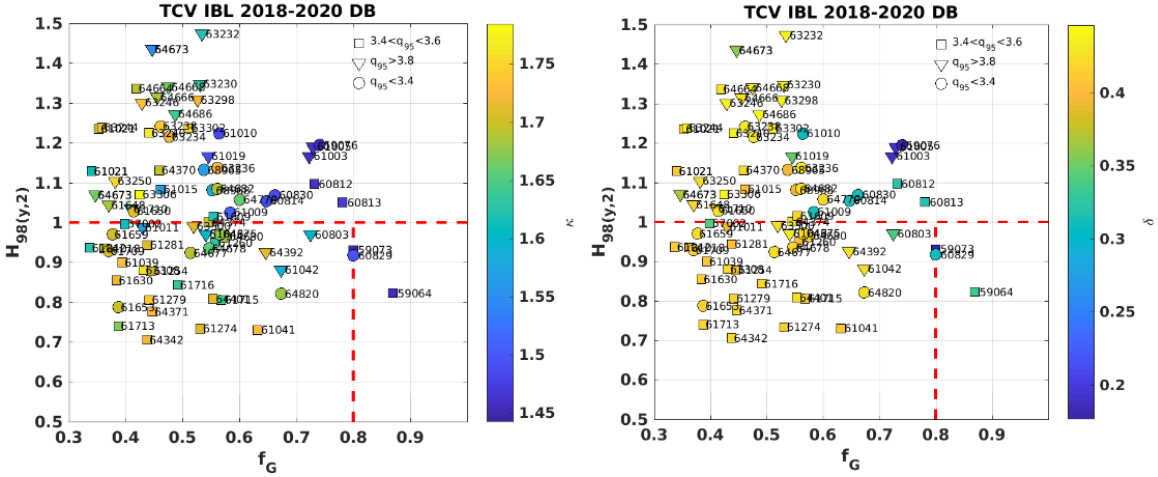

FIG. 4: *H_{98} vs f_G for our present ITER-like shapes, including k>1.45 and d>0.18. Colors according to (a) κ and (b) δ.*

On the other hand, density peaking is usually consistent with an ITG dominated regime (see below) and better confinement. Since the AUG low collisionality cases span the same region in (β_N, H_{98}) as the TCV good confinement, high q_{95} cases, we compare in Fig. 5 the density profiles of two AUG discharges: 35564 (standard IBL q_{95}~3) and 34841 (low ν*, q_{95}~3.6). The low ν* case is clearly much more peaked than the standard AUG IBL cases and can explain the good confinement properties despite the edge pump-out effect.

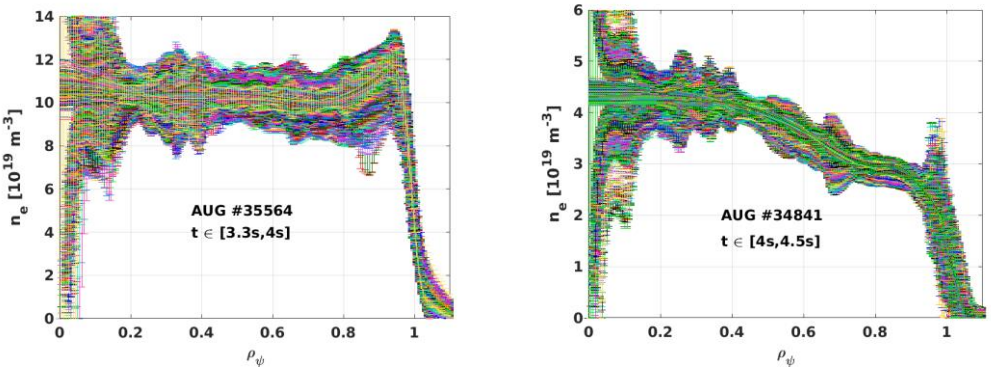

FIG. 5: n_e profiles in AUG IBL for (a) standard q_{95}=3 and (b) q_{95}=3.6, low ν* with edge pump-out thanks to MP coils

3. ROLE OF MHD AND DURATION OF HIGH PERFORMANCE

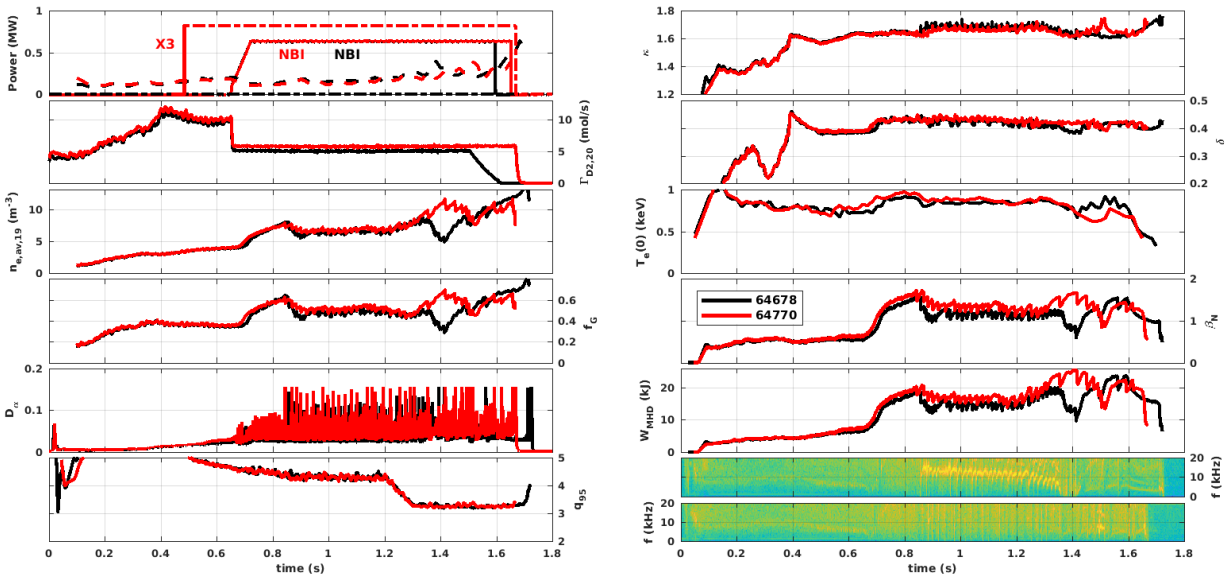

FIG. 6: *Time traces of two TCV IBL discharges with (64770, red) and without (64678) X3 central EC heating. A 2/1 mode is triggered at 0.86 in 64678 at the first large ELM, while only a small n even mode at ~40kHz appears in 64770. Later 64770 has a short lived 2/1 at 1.5s yielding low β and mode self-stabilization. Similarly for 64678, the 2/1 mode locks at 1.35s, yields an H-L back transition and self-stabilizes. The discharge goes quickly back to good type I ELMy H-mode*

Neoclassical tearing modes are very often observed in these TCV IBL scenarios, usually 3/2 or 2/1 modes which can lock and unlock depending on the plasma profiles evolution. They can be triggered by the large ELM crashes, which have ΔW/W~20%, or be born as tearing modes, or "both" in most cases. "Both" because tearing modes are more unstable with a broad current density profile and therefore can more easily be made unstable by external perturbations. In TCV IBL, the density peaking is significant, especially when comparing with usual AUG cases. This leads to flat and broad T_e profiles, often the loss of sawteeth (q>1), and therefore broad current density profiles. Similarly to density limits, core impurity accumulation or hybrid scenarios, these resulting current density profiles tend to be more prone to tearing modes. We have tested the role of input power and electron heating in a series of otherwise similar discharges with a first phase at high q_{95} (~4.2 from 0.8-1.2s) and a 2nd phase with q_{95}~3.2 from 1.3-1.7s. In the first discharge, 64678, shown in black in Fig. 6, a 2/1 mode appears in the 1st phase and degrades the confinement. On the other hand, adding X3 heating, as in the 64770 shown in red, avoids this mode onsets, although a similar 1st big ELM occurs, but only an even n at ~40kHz is triggered (small 3/2) which disappears when I_p is increased at 1.2s. The 2/1 can lock as here at 1.35s in 64678, which usually leads to

significant confinement degradation and an abrupt H-L back transition which can lead to disruption. It can also lead to a sufficient drop in beta and profiles such as to stabilize the NTM, after which the discharge recovers quickly. Note that the confinement time is τ_E~20-30ms, therefore TCV IBL are sustained for ~5τ_E for q_{95}~3.2 and >10τ_E for q_{95}>3.6. As seen for the 64770 near 1.4s, the low q_{95} phase has high β_N for a few ELM periods, until a mode is triggered. Since the ELM period is 40-60ms, about 2-3 τ_E this is the main limitation for the high performance duration. Note that the current redistribution time is short on TCV, about 100ms, hence it is long in this respect. This may explain the large perturbation caused by the ELM crash and consistent occurrence of 2/1 modes after a few ELMs, as observed in [11].

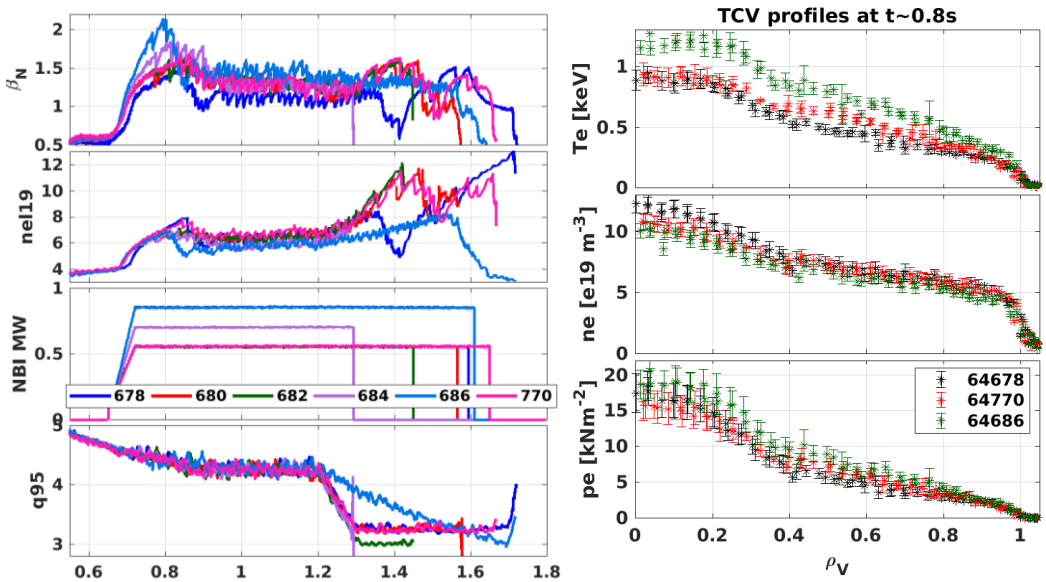

FIG. 7: (a) *Sequence of discharges with increasing NBI power and different Ip ramps in the later phase. All the shots except 64678 have X3 ECH (0.8MW injected, ~0.2MW absorbed in early phase). Note that only about 10-15% of the NBI power goes to electrons, and twice as much to ions in the first phase. At higher current and density, in last phase twice these values apply. 64770, 64680 and 64682 do not have 2/1 modes in early q_{95}~4.2 phase. (b) Profiles at 0.8s*

Let us focus on the early high q_{95} phase, 0.8-1.2s, of these discharges. We have repeated 64680 and 64682 with X3, which both also do not trigger the 2/1 mode, then higher NBI power 64684 and 64686, as shown in Fig. 7a, still with X3, which triggered 2/1 modes near the 5th and 2nd ELM crash, respectively, at β_N~1.8 and 2.1. Therefore at β_N>1.65 we could not avoid the 2/1 NTM with X3 and q_{95}~4.2, while at β_N~1.6 it is sufficient. Comparing the profiles without/with X3 (64678 black/64770 red) in Fig. 7b, we see that the density is more peaked in the former case. On the other hand, at β_N~2.1, T_e is much higher (green) with a similar density profile as 64770 and a 2/1 mode is triggered. Moreover, in the later phase with q_{95}~3.2 a 2/1 mode is triggered at β_N~1.6 and with X3, although the X3 coupling is much smaller due to the higher density (n_{e0}~1.5e20>cut-off) and lower T_e. These cases and other shots not shown here confirm that it is the combination of high β_N, peaked density profile, high elongation and large ELMs which consistently leads to the triggering of 2/1 modes after a few ELM crashes.

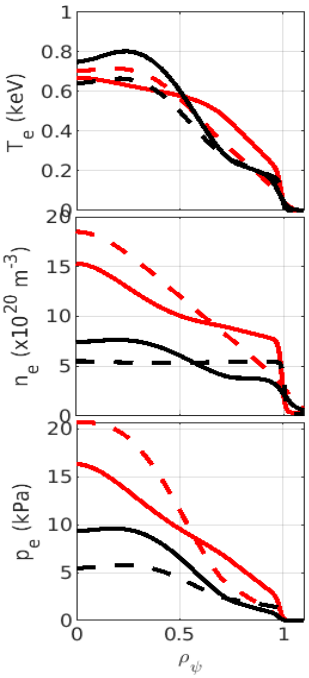

(dashed) ELM crash at 1.4s for 64770 (red), without modes and 64678 (black with a locked 2/1 mode.

In the later phase, increasing plasma current to reach q_{95}~3, β_N remains high or even increases. This is due to the fact that density also increases and NBI coupling is usually better with less 1st orbit and mainly CX losses [13]. Note that we did not remove the CX loss in the computation of the H_{98} factor, in order to be conservative. This leads typically to a 10-20% underestimation. In order to complete the comparison of the effects of modes and ELMs on the profiles, we show in Fig. 8 the profiles before and after an ELM crash at 1.4s in the two shots presented in Fig. 6. The shot 64770 is one of our best performance shot, with κ~1.66, δ~0.42, β_N~1.7, H_{98}~1 and f_G~0.65. The pre- and post-shot profiles (red and magenta in Fig. 8) show that the profiles are modified up to essentially mid-radius. The 64678 has a locked 2/1 mode, explaining the large difference in pressure in otherwise similar conditions (only about 80kW X3 EC not injected in 64678).

Nevertheless the relative effects on the profiles (black to green) is large and over the whole plasma radius, explaining how it can lead to an unlocking (at 1,42s) and self-stabilization (at 1.43s) of the mode.

4. AUG IBL SAFE TERMINATION

In the recent campaign, progress has been obtained related to the safe ramp-down of IBL scenarios in AUG. Integrated modelling of AUG discharges including the ramp-down phase has been performed using the RAPTOR code [14] and then an optimization procedure for the termination phase has been conducted, also described in [14]. The main ingredients for a safe and yet rapid termination are a decrease of plasma current together with a decrease of elongation, while controlling the heat sources during the whole termination. The goal being to trigger an H-L transition at about 1/3 of the ramp-down, the elongation should not decrease too fast, in order to avoid too low q_{95} values, and the H-L transition should not occur too late to avoid a too large Greenwald fraction. These key ingredients allow a control of the l_i time evolution, elongation and power balance. These studies have also been used to develop the real-time termination algorithm used in JET baseline scenarios [15]. The simulation results were then used to design the termination segment for IBL scenarios. An example is shown in Fig. 9, where a high current case safely ramps down to 0, with a controlled H-L transition, in this case when power is turned off, about 1/3 into the ramp-down and an elongation decreasing while decreasing I_p. This leads to a slow increase of the internal inductance and a stable plasma. All IBL scenarios using this segment terminated in a safe way.

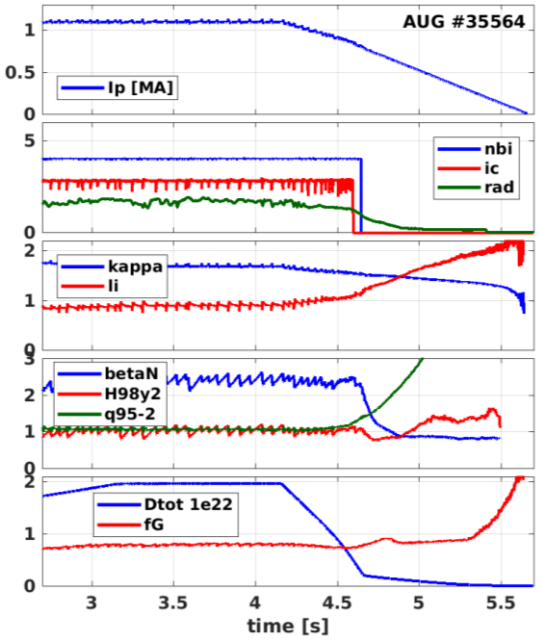

FIG. 9: AUG q_{95}=3 IBL with a safe termination including H-L timing and $\kappa(t)$ control.

5. TRANSPORT MODELLING OF TCV ITER BASELINE SCENARIOS

The capability of a quasi-linear drift mode based transport model to predict the thermal and particle transport in TCV ITER baseline scenario is examined here for two discharges, one at q_{95}~3.2 (64770) described in the previous section and one at q_{95}~3.7 (alternative IBL 63306). The evolution of electron (T_e) and ion (T_i) temperatures and main ion (n_D) as well as the poloidal field diffusion equation are simulated in the whole plasma region (ρ=0-1) with ASTRA code [16] starting in the ohmic phase (0.5s) and finishing at the end of the high plasma current flat-top. The NBI simulations are performed self-consistently with plasma evolution taking into account the shine-through, CX and orbit losses, while the TORAY-GA code [17] is used for the ECRH/ECCD modelling performed with the measured plasma profiles. The transport model applied here combines the GLF23 [18] computed transport coefficients in the core region (ρ=0-0.85) with ad-hoc edge transport coefficients and NCLASS [19] used for the thermal and particle transport as well as current conductivity and bootstrap current. The GLF23 model is used here as a numerically fast approximation to TGLF which allows to simulate the entire scenario in a computationally reasonable time while providing important information on the microturbulence stability and the effects potentially stabilising anomalous transport. The impact of observed sawtooth oscillations is taken into account by increasing the transport coefficients within mixing radius simulated self-consistently with the q-profile evolution assuming the Kadomtsev reconnection model. In addition, the feedback control of the volume averaged density via the neutral influx is applied. In the absence of T_i measurements the diamagnetic energy W_{dia} extracted from the diamagnetic flux measurements and consistent with the LIUQE [20] equilibrium reconstruction has been used for comparison with W_{dia} obtained in transport modelling.

The measured and simulated electron density and temperature profiles are shown in Fig. 10. Self-consistent transport simulations show that ITG is the dominant instability in a broad plasma region ($\rho \cong$0.3–0.8) during the quasi-stationary phases achieved at the I_p flat-top, with a narrow inner TEM-dominant region (at $\rho\cong$0.2–0.3). These results are consistent with the linear microturbulence stability analysis performed with GENE [21] for one of analysed discharges (Fig. 11). The T_e and n_e evolution in discharge 64770 gives an indication of strong electron temperature stiffness – both simulated and experimental electron temperature weakly evolve during the discharge in spite of the strong density increase (Fig. 10, bottom panels) and reduced auxiliary electron heating from 0.25MW at 1.2s to 0.16MW at 1.4s (somewhat overestimated) – mainly due to a reduced ECRH absorption at high density. Similar results, i.e. dominant ITG-driven anomalous transport in the broad region around mid-radius well predicting the measured T_e profiles and stiff electron temperatures have been obtained also in the thermal

transport modelling of four other TCV IBL discharges covering a broad parameter space (n_{e0} = (4.5-10) $10^{19}m^{-3}$, NBI, ECRH and combined NBI and ECRH heated plasmas) [21].
Two discharges analysed here are characterised by strong density peaking reasonably predicted up to the central density values of (10-12) $10^{19}m^{-3}$ and slightly underpredicted at higher n_e (#64770, 1.4s). It should be mentioned that the drift modes are stable within ρ=0.2 in performed simulations and the transport in the central region is determined by NCLASS enhanced by the sawteeth mixing. A relative contribution of the central (NBI) vs wall sources to plasma fuelling and density peaking is investigated for discharge 63306 in the self-consistent density, temperature and current diffusion simulations by switching off one of these sources at 1.185s in separate simulations, freezing all input parameters at this time and continuing the simulations with the remaining particle source till stationary state. The stationary density profile obtained with the NBI fuelling only and with the wall source only are shown by blue and red curves in Fig. 10 (top left panel). The density pedestal is reducing in the absence of wall particle source causing a density reduction deeper in the plasma region, but the central density is still well maintained by the central NBI fuelling (case shown by blue curve). A much larger density reduction is obtained when the NBI fuelling is switched off (red curve) showing that the NBI particle source plays a larger role in plasma fuelling. However, the density profile is strongly peaked in each single source simulation. In case of wall fuelling this peaking is fully provided by the drift mode stability in the plasma centre, but in all other simulations the reduced transport in the central region also plays role in the density peaking.

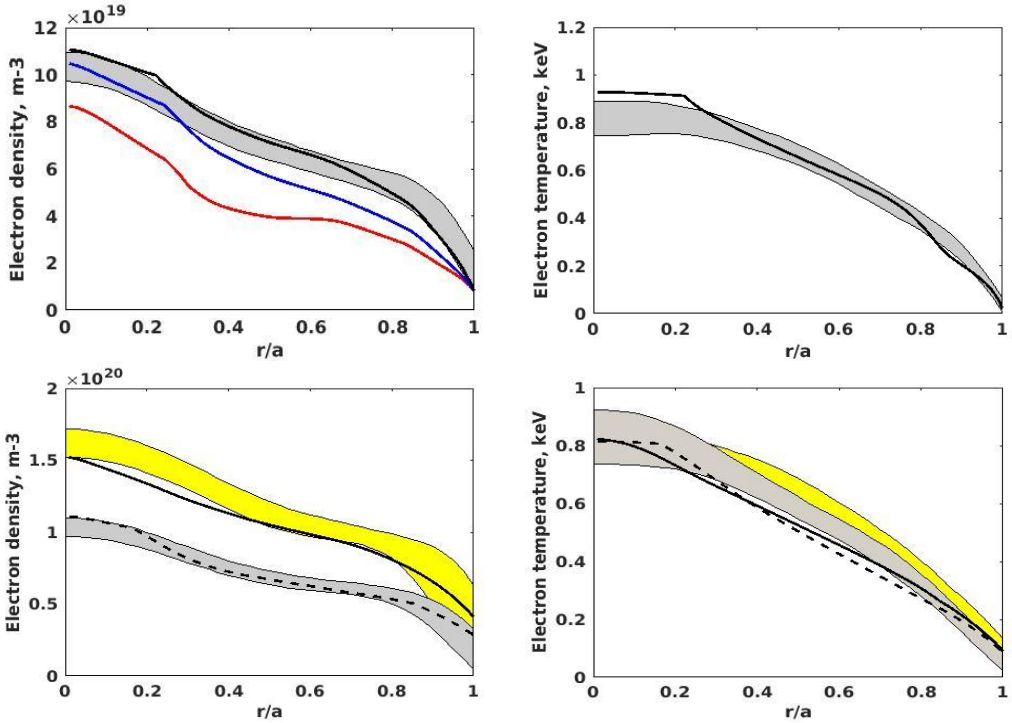

FIG. 10. Simulated n_e (left) and T_e (right) profiles in TCV IBL discharges 63306 (top, 1.185s) and 64470 (bottom, 1.2s (dashed) and 1.4s (solid)). Colour curves on the top left panel show the stationary density profiles achieved with NBI particle source only (blue) and wall neutral source only (red) fixed at 1.185s. Grey areas indicate the experimental profiles with error bars. $W_{dia,exp}$=23kJ, $W_{dia,sim}$=22.3kJ at 1.185s in 63306. $W_{dia,exp}$=16.8kJ, $W_{dia,sim}$ =16kJ at 1.2s and $W_{dia,exp}$ =25.2kJ, $W_{dia,sim}$ =24.9kJ at 1.4s in 64770.

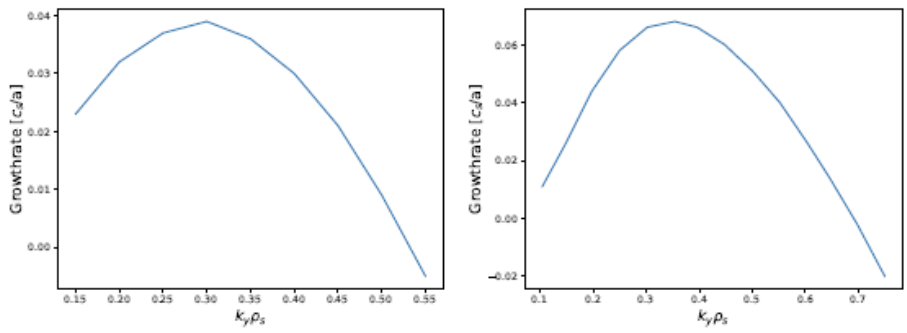

FIG. 11. Microturbulence growth rates at mid-radius in AUG #36143 (left) and TCV #64770 (right) using GENE, finding ITG as most unstable mode in both cases.

6. CONCLUSIONS

TCV ITER baseline scenarios have been successfully developed and analysed within the EUROfusion WPMST1 campaigns, starting first with a similar shape as the AUG IBL and then moving towards higher edge triangularity and elongation. TCV spans the ITER target values (H_{98}~1, β_N~1.8 at q_{95}~3 and H_{98}~1.2, β_N~2.2 at q_{95}~3.6), and slightly better confinement properties, consistent with previous findings with carbon wall. Integrated modelling using ASTRA-GLF23 quasi-linear drift mode based transport model predicts the observed heat and particle transport, with ITG dominant regime in most of the radial extent. In particular, it also predicts the mainly turbulent-driven significant density peaking observed in TCV IBL discharges. AUG IBL cases with similar good confinement properties, at low ν^*, also exhibit density peaking contrary to the standard AUG IBL discharges. The TCV IBL high performance and low q_{95} cases are limited by the occurrence of 2/1 modes, occurring typically after 1-2 current redistribution time, which is only a few ELM periods in TCV. It has been shown that broad current density profile, induced by density peaking, as well as elongation, high β_N and low q_{95} combine to lead to more unstable plasma to "both" classical and neoclassical tearing modes. Both in the sense that these combined parameters lead to more unstable q profiles to classical tearing onset, and to larger perturbation due to type I ELMs. TCV IBL can avoid these modes at medium β_N and/or high q_{95} with X3 EC heating, and also at lower elongation. We have also shown that lower elongation helps in reaching IBL discharges at high Greenwald fraction. We have used the benefit of controlled elongation and power source during AUG IBL termination phases (in feedforward). Safe ramp-down scenarios, inspired by off-line optimization results using RAPTOR, have been demonstrated on AUG including the q_{95}=3 scenario. The combination of I_p and κ ramp-down with a pre-defined H-L transition timing keeps the time evolution of l_i and of the density within a safe operating range. Contrary to the flat top part, where high elongation leads to low l_i and more unstable profiles, in the ramp-down phase too high l_i needs to be avoided. Note that both can lead to higher magnetic shear near q=2, similar to impurity accumulation or edge cooling respectively. Analyses will be continued to test this overall consistent picture.

ACKNOWLEDGEMENTS

This work has been carried out within the framework of the EUROfusion Consortium and has received funding from the Euratom research and training programme 2014 - 2018 and 2019 - 2020 under grant agreement No 633053. The views and opinions expressed herein do not necessarily reflect those of the European Commission. This work was supported in part by the Swiss National Science Foundation.

REFERENCES

[1] SIPS A. C. C. et al, Nucl. Fusion **58** (2018) 126010
[2] PÜTTERICH T. et al, 2018 IAEA FEC, IAEA-CN-EX/P8-4
[3] FASOLI A. et al, Nucl. Fusion **49** (2009) 104005
[4] SHIMADA M. et al, Nucl. Fusion **47** (2007) S1
[5] MERLE A. et al, Plasma Phys. Control. Fusion **59** (2017) 104001
[6] SCHWEINZER J. et al, Nucl. Fusion **56** (2016) 106007
[7] SUTTROP W. et al., Fusion Engineering and Design **84** (2009) 290
[8] MANTSINEN M. et al, this conference IAEA 2021, paper IAEA-EX/P3-, IAEA-CN-991
[9] LABIT L. et al, this conference IAEA 2021, IAEA- EX/P4-17, IAEA-CN-883
[10] REIMERDES H. et al, Plasma Phys. Control. Fusion **48** (2006) 1621
[11] TURCO F. et al, Nucl. Fusion **58** (2018) 106043
[12] KONG M. et al, Nucl. Fusion 60 (2020) 026002
[13] GEIGER B. et al, Plasma Phys. Control. Fusion **59** (2017) 115002
[14] TEPLUKHINA A. A. et al, Plasma Phys. Control. Fusion **59** (2017) 124004; PhD thesis No 8478, EPFL, Lausanne, 2018
[15] SOZZI C. et al, this conference, IAEA 2021, paper IAEA-CN-978
[16] PEREVERZEV G. V. AND YUSHMANOV P. N., IPP Report 5/98 (2002) and FABLE E. et al, PPCF **55** (2013) 124028
[17] MATSUDA K. IEEE Trans. Plasma Sci. **17** (1989) 6
[18] WALTZ R.E. AND MILLER R.L. Phys. Plasmas **6** (1999) 4265
[19] HOULBERG W.A. et al, Phys. Plasmas **4** (1997) 3230
[20] MORET J.M. et al, Fusion Eng. Des. **91** (2015) 1
[21] JENKO F. AND DORLAND W., Plasma Phys. Contr. Fusion **43** (2001) 12A
[22] VOITSEKHOVITCH I. et al, private communication, https://iterphysicswiki.euro-fusion.org/images/d/da/TCV_IBL_modelling_Irina.pdf